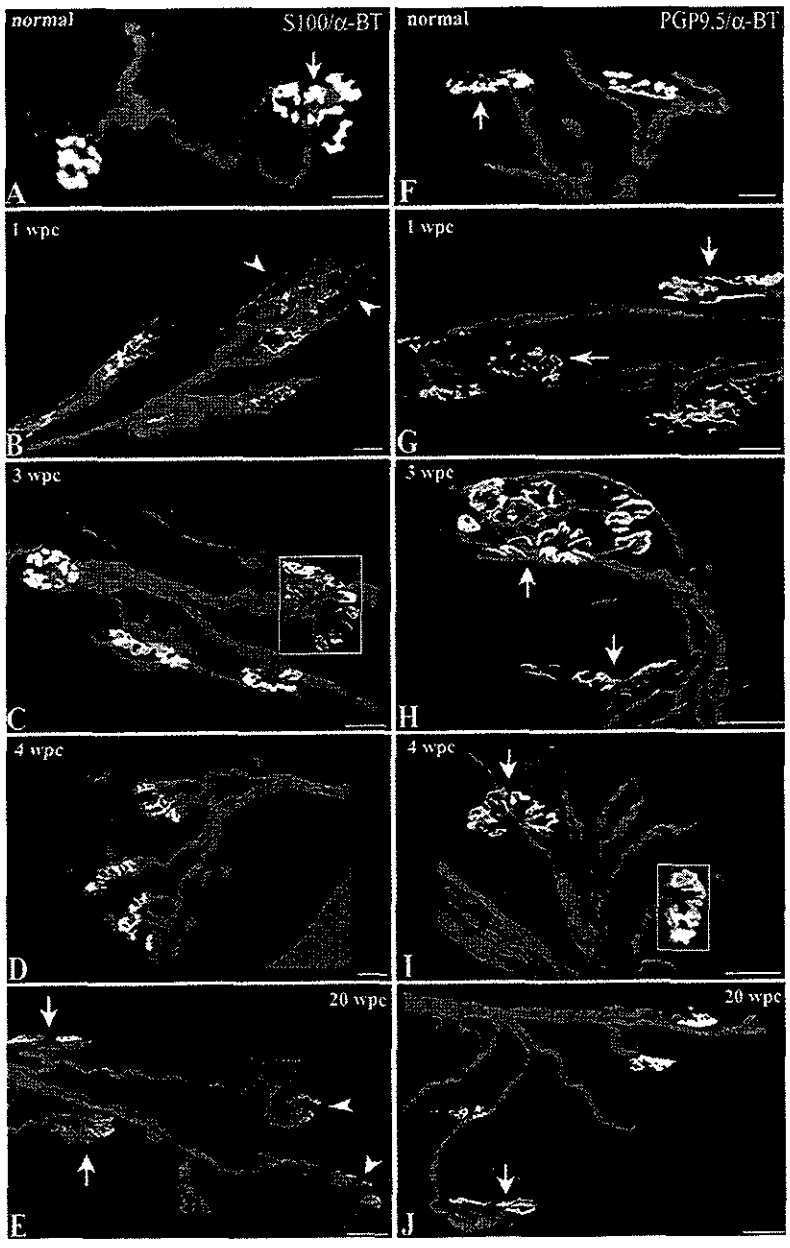

Figure 3. (A–E) Double-fluorescence labeling for S100 (red) and α-BT (green) in longitudinal sections of neuromuscular junctions (NMJs) at unoperated control (A), 1 (B), 3 (C), 4 (D), and 20 (E) weeks post-crush (wpc), and (F–J) double fluorescence labeling for PGP9.5 (red) and α-BT (green) at control (F), 1 (G), 3 (H), 4 (I), and 20 (J) wpc show the sequence of endplate reoccupation by S100-positive terminal Schwann cells (TSCs) and PGP9.5-positive axon terminals. The superimposed red and green images show superposition areas that appear yellow between SCs/axons and postsynaptic acetylcholine receptor (AchR) plaques. Note in all figures that TSCs or axon terminals invariably regenerate within the territory of AChR geometry. (A, F) NMJs (arrows) in unoperated controls. Note almost complete and accurate spatial occupation between nerve terminals [TSCs (A), axon terminals (F)] and postsynaptic receptor regions. (B) Loosely aligned TSCs with profuse robust extensions (arrowheads) overlie AChR sites with degeneration figures (*shrinkage, fragmentation*). (C–E) In most NMJs, TSCs are well organized and aligned with regular contours, indicating ongoing regeneration. (C, D) From early in reinnervation, the yellow-colored superposition predominates, indicating that the major area of the TSC profile closely contacts over the area of the AChR plaque. (E) At 20 wpc, some NMJs show almost complete superposition (arrows), while in others (arrowheads), less developed TSCs are coupled with poorly formed AChR plaques. (G) At 1 wpc, axon terminals are disorganized and disintegrated in a majority of NMJs, with AChR plaques being left unoccupied (arrows). (H–J) With advancement of endplate reoccupation, the terminal arborizations expand into a series of boutons and cover the entire NMJ area. (H, I) Early in reinnervation, *superposition of the axon terminals* and AChR sites (arrows) is seen. (J) At 20 wpc, despite advancement in superposition, poorly formed terminals, partially occupying an AChR plaque, still can be seen (arrow). The boxed regions in (C) and (I) were processed in Fig. 2. Scale bar = 20 μm.

measured. To minimize the subjective bias in delineation of the borders of the structure, the scope of the gray image was always referenced to that of the original color image (green, red, or yellow). Following measurement of the superimposed yellow area, the ratio of CC at 4, 8, 12, and 20 wpc was estimated by the quotient of the mean area of the yellow image divided by the green-colored AChR sites. Morphometric analyses of characters and relationship among three components of NMJ during muscle reinnervation were always referenced to the normal controls and were performed independently by two investigators on original images. Their results were compared to evaluate accuracy.

Statistics

The incidence of anomalous changes in TSCs and axon terminals, as expressed by a percent, were compared with the chi-square test at a level of significance of 99%. For the superposition areas delimited by TSCs or axon terminals, mean and standard deviations were calculated. Differences in the means of each parameter at 4, 8, and/or 12 wpc were compared with a two-tailed Student's *t*-test. Differences between the two values were considered significant if the probability value (p) was found to be less than 0.05.

Results

Correlation in size between presynaptic and postsynaptic elements

Nerve crush induced long-lasting atrophy of AChR sites in which their area, perimeter, and diameter significantly reduced from normal levels, and the degree of reduction in the area of the AChR site was prominent at 4 wpc, with subsequent restoration at 12 wpc *(Kawabuchi et al., 2001)*.

The distribution of individual value pairs of the areas of TSCs and AChR sites is shown by the scatter diagrams (Fig. 1A–C). A positive relation was most evident in controls, and sizes of AChR sites were significantly correlated with those of TSCs in controls [the correlation efficient (r) for endplate area and TSC size = 0.94, $p < 0.001$] (Fig. 1A). Across all the time points (4, 8, and 12 wpc), significant correlation was maintained during reinnervation following nerve crush ($r = 0.42$ at 4 wpc, $p < 0.001$; $r = 0.85$ at 8 wpc, $p < 0.001$; and $r = 0.33$ at 12 wpc, $p < 0.01$) (Fig. 1B,C). The area of most AChR sites decreased at 4 wpc and gradually recovered to the normal level. Compared with the decrease in the area of AChR sites, some areas of TSCs increased and the others decreased at 4 wpc. The relationship between both gradually became correlated as shown in the control.

At the same time, sizes of AChR sites were also significantly correlated with those of axon terminals (r for endplate area and axon terminal size = 0.93, $p < 0.001$) (Fig. 1D). The area of most axon terminals decreased with the decrease in AChR sites at 4 wpc. During muscle reinnervation, the increase in area of axon terminals obviously correlated with area of postsynaptic receptor region ($r = 0.86$ at 4 wpc, $p < 0.001$; $r = 0.54$ at 8 wpc, $p < 0.001$; and $r = 0.75$ at 12 wpc, $p < 0.001$) (Fig. 1E,F). The proportion of the small-sized axon terminals/AChR sites predominated at 12 wpc.

Anomalous superposition between TSCs (or axon terminals) and AChR sites in NMJs

During 4–20 wpc, we note that the magnitudes of endplate reoccupation between the pre- and postsynaptic sites greatly varied in NMJs, and some anomalous superposition figures emerged either accidentally or in groups within the muscle (Fig. 4A–I). For TSCs, we note that 1) regenerating TSCs overlapped either well-organized (Fig. 4C) or shrunken (Fig. 4F) AChR sites and 2) some of the AChR plaques showed signs of undifferentiation, such as flat, less intensely stained, and often wider than initially seen, without branching or segmentation to delineate the synaptic invaginations (Fig. 4I).

Uncoordinated spatial alignment in each of the disorderly regenerating axon terminals was a consistent feature (Fig. 5A–L), aside from those with complete reoccupation and close superposition (Fig. 5M–O). We note that major anomalous changes consisted of superposition of regenerating axon terminals with shrunken and less-developed AChR sites (Fig. 5A–F). In some NMJs, the branching area of the nerve terminal was great enough, but its greater part was not overlapped with the AChR site (Fig. 5A–C). At the same time, some AChR sites displayed were only partially occupied (Fig. 5D–F). (2) During this period, polyaxonally innervated NMJs were frequently found, including multiple extensions traveling through the same pathway into the same NMJ and sharing it. Each axon terminal sharing the same multiple innervated NMJ displayed similar but no identical pattern of superposition (Fig. 5J–L).

Statistics for incidence of anomalous superposition per junction

'Anomalous change' was defined as NMJs with greatly unoccupied AChR plaques with occupation ratios less than 50% and/or poorly formed endplate occupants. The time courses of number of anomalous changes per junction are shown in Fig. 6. The number of the TSC-related anomalous changes peaked at 4 and 6 wpc, with a subsequent later decline (Fig. 6A). In contrast, the incidence of anomalous axon

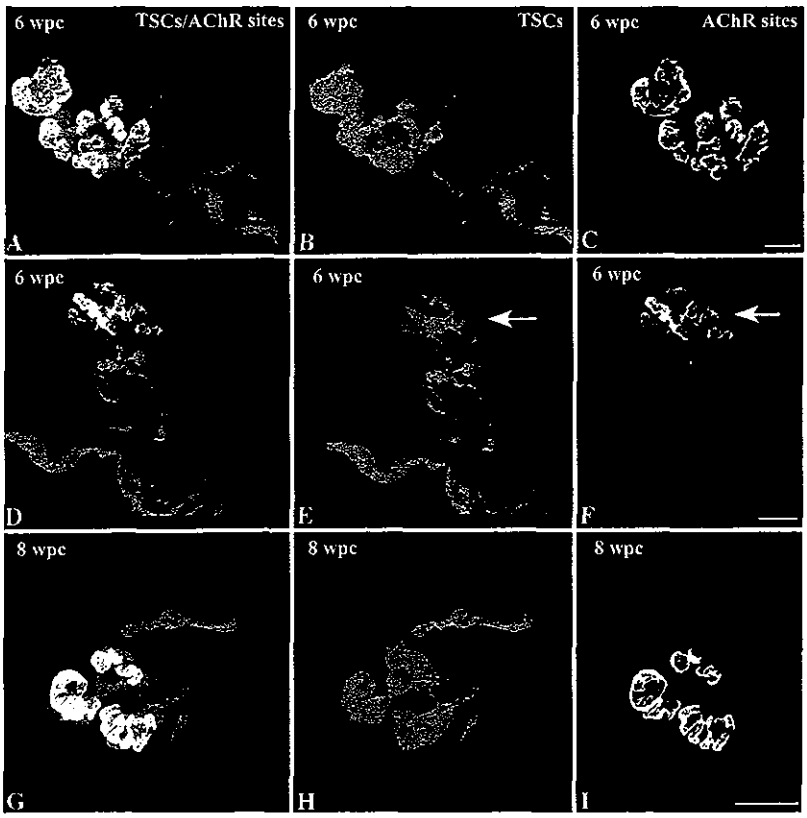

Figure 4. Anomalous figures during endplate realignment of terminal Schwann cell (TSC)/acetylcholine receptor (AchR) site at 6-weeks post-crush (wpc) (A–C, D–F) and 8 wpc (G–I). A, D, G: superimposed images. B, E, H: TSC profiles. C, F, I: AChR sites. (A–C) Ongoing endplate superposition is displayed between the TSC and AChR site. (D–F) Poorly developed TSCs are superimposed with poorly formed AChR sites, which manifest thin flat plaques and ill-defined contours (arrows). (G–I) TSCs with well-defined shapes and edges overlap an AChR plaque showing the lack of the usually segregated organizations, suggesting shallow branching and undeveloped synaptic infoldings. Scale bar = 20 μm.

terminal-related superposition displayed biphasic changes, peaking in the early (4 wpc) and late (12 and 20 wpc) reinnervation periods. The latter change was possibly derived from remodeling or adaptation of regenerating NMJs (Fig. 6B).

Delay in CC between axon terminals and AChR sites in NMJs during muscle reinnervation

In unoperated controls, the superimposition of nerve terminal staining over AChR sites showed that there was almost complete spatial occupation between nerve terminals and postsynaptic receptor regions, with very few pre- (the nerve terminal extending beyond the post-projection) or postsynaptic displacement (post-projection extending beyond the nerve terminal) (Fig. 3A,F).

Labeling for S100 in NMJs at 1 wpc clearly defined chain-like cellular strands as regenerating SC strands, and the junctional clusters of round or elliptical cells with profuse process extensions as TSCs (Fig. 3B). These TSCs overlapping AChR plaques mostly showed features of degeneration such as shrinkage and fragmentation. At 3 wpc, greater portions in regions of CC between the TSCs and AChR plaques displayed green-colored FITC fluorescence, indicating that S100 labeling only partially covered the area of AChR plaques at the NMJ (Fig. 3C). From 4 wpc, most NMJs became yellow-colored, where coverage of TSCs over the area of AChR plaques is almost complete (Fig. 3D–E). This endplate profile showed a consistent feature until 20 wpc, while fewer developed TSCs superimposed with fewer developed AChR plaques still persisted in some NMJs (Fig. 3E).

Comparison of the axon terminal-mediated superposition with that of TSCs indicated that the way in which the axon terminals branched to occupy the AChR sites was different. At 1 wpc, there was no or sparse labeling for PGP9.5 in NMJs, with only vacant AChR plaques being left (Fig. 3G). During 3–20 wpc, reoccupation of the axon terminals over the AChR plaques was in process. At 3 and 4 wpc, greater portions in regions of CC between the axon terminals

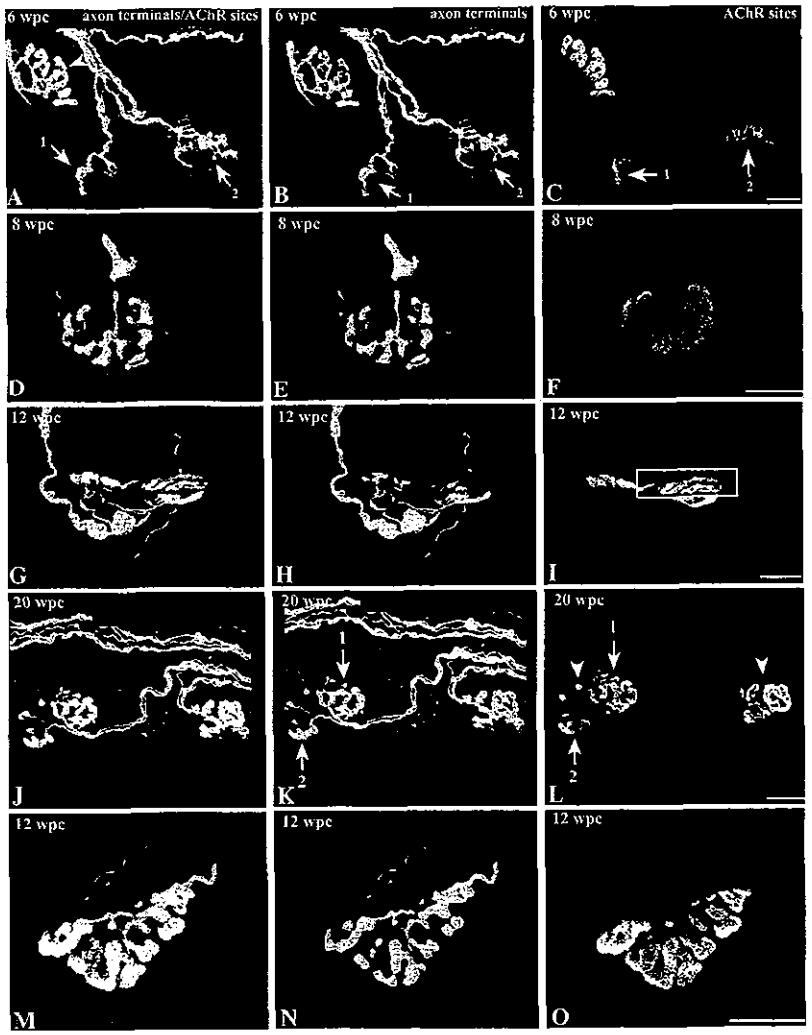

Figure 5. Anomalous changes during endplate realignment of axon terminal/acetylcholine receptor (AchR) site at 6- (A–C), 8- (D–F), 12-(G–I, M–O), and 20-weeks post-crush (wpc) (J–L). A, D, G, J, M: superimposed images. B, E, H, K, N: axon terminals. C, F, I, L, O: AChR sites. (A–C) Besides normally occupied neuromuscular junctions (NMJs) (arrowhead), there is a wide variability in degree of superposition at poorly developed NMJs. In the two junctions (arrows 1 and 2), well-developed terminal arbors greatly contrast with the poorly formed AChR plaques. (D–F) Regenerating terminal arbor overlaps an AChR plaque manifesting granular distribution with the frayed border. (G–I) The boxed region of an AChR plaque, displaying shrinkage and simplicity, remains unoccupied by the axon terminal, indicating discrepancy in sizes of individual endplate occupants. (J–L) Superposition patterns from polyaxonally innervated NMJs, where two or more extensions travel up the same course to the NMJ. Multiple innervated NMJs show well-regenerated terminals, while individual terminal plaques sharing the same NMJ (arrows 1 and 2) display similar though not identical superposition patterns. (L) The simplified structures (right arrowhead) and a few small round or spindle-shaped plaques (left arrowhead) in AChR sites are estimated as signs of reconstruction. (M–O) Fully regenerated anatomical relations in the later reinnervation period. Scale bar = 20 μm.

and AChR plaques mostly displayed green-colored FITC fluorescence, indicating that axon terminals only partially occupied the limited area of AChR plaques (Fig. 3H–I). Progressively, more area of the postsynaptic receptor region was covered by well-defined and elaborate arborizations of axon terminals, and endplate reoccupation was almost complete in 90% of the NMJs at 20 wpc (Fig. 3J).

Statistics for area of CC per junction

The rates of increase in the extent of superposition areas that follows reinnervation were not proportionate between TSCs and axon terminals (Fig. 7). The pattern of CC of the TSCs or axon terminals in unoperated controls was similar to that seen in the sham controls. At 4 wpc, the mean superposition areas of the TSCs compared with mean control values showed a 20% increase (158/131, $p < 0.001$, *t*-test); however, those

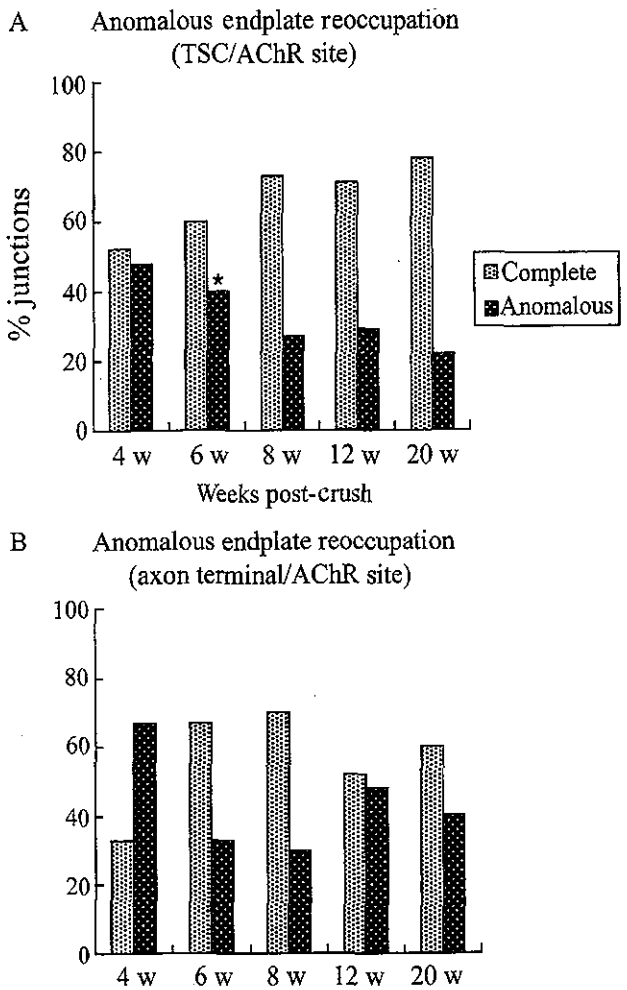

Figure 6. Bar graphs showing time courses of the incidence of anomalous changes during endplate reoccupation, such as greatly unoccupied endplates and/or less developed occupants. The incidence, in respect to the total number of neuromuscular junctions (55–90), was measured. (A) As for the number (mean percent) of anomalous changes per terminal Schwann cell-apposing junction, the peak at 4-weeks post-crush (wpc) and 6 wpc shows a subsequent decline (6 vs. 8, 12 or 20 weeks, *$p < 0.001$, chi-square test). (B) In the axon terminal-apposing junctions, the anomalous incidence shows the prominent rise in the early (4 wpc) and late reinnervation period (12 and 20 wpc).

of the axon terminals decreased by 45% (73/162, $p < 0.001$) (Fig. 7A,B). For TSCs, the increases with a subsequent decline to normal level during the period suggest that regenerating TSCs attained wider superposition areas than in controls, besides rapidly restoring contact areas to the postsynaptic receptor regions. But compared with TSCs, it was remarkable that the mean superposition areas of regenerating axon terminals were consistently smaller than controls, with gradual return to control levels [81% (125/154) at 8 weeks and 86% (155/180) at 20 weeks] (Fig. 7B).

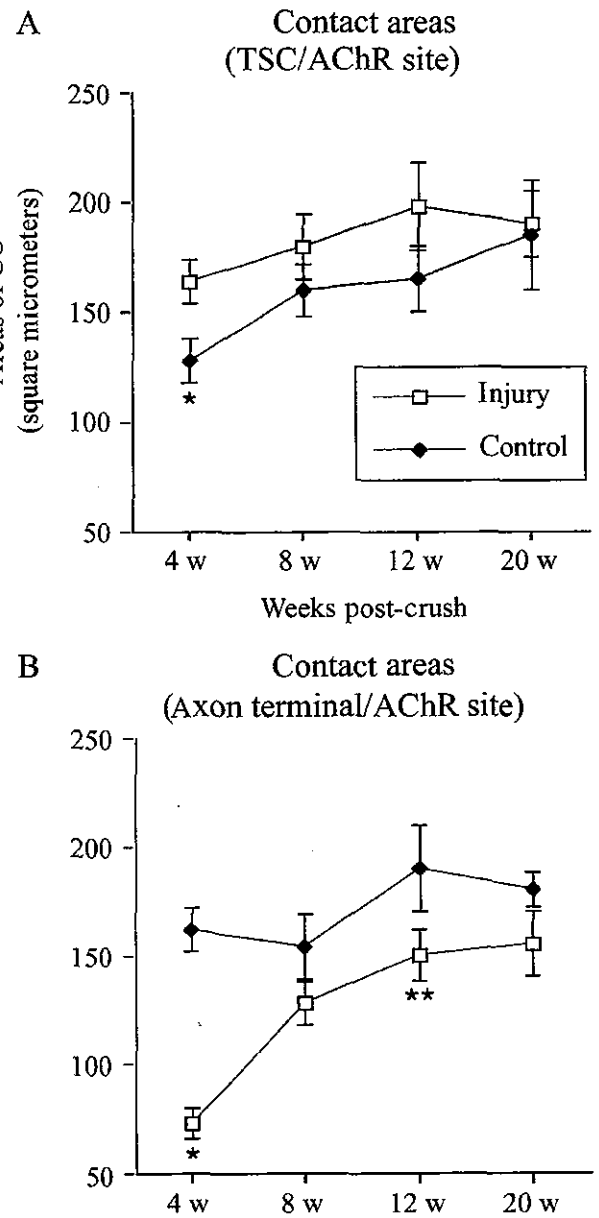

Figure 7. Extent of close correspondence (CC) delineated by terminal Schwann cells (TSCs) (A) or axon terminals (B) at 4-, 8-, 12-, and 20-weeks post-crush (wpc). Values (μm^2) are expressed by the mean area ± standard error of CC among the total number of junctions. A total of 60–75 junctions were evaluated per time point. (A) Compared with controls, contact areas of TSC/acetylcholine receptor sites show increases until 20 wpc, possibly due to growth and remodeling of junctions. Values at 4 wpc already are over normal levels (control vs. 4 wpc, *$p < 0.025$) and at 20 wpc recover to normal levels. (B) As compared with controls, areas of axon terminals show decline, especially at 4 (*$p < 0.025$) and 12 wpc (**$p < 0.05$).

Statistics for ratio of CC per receptor region

The time courses of the ratios of CC delimited by TSCs or axon terminals to the geometry of AChR

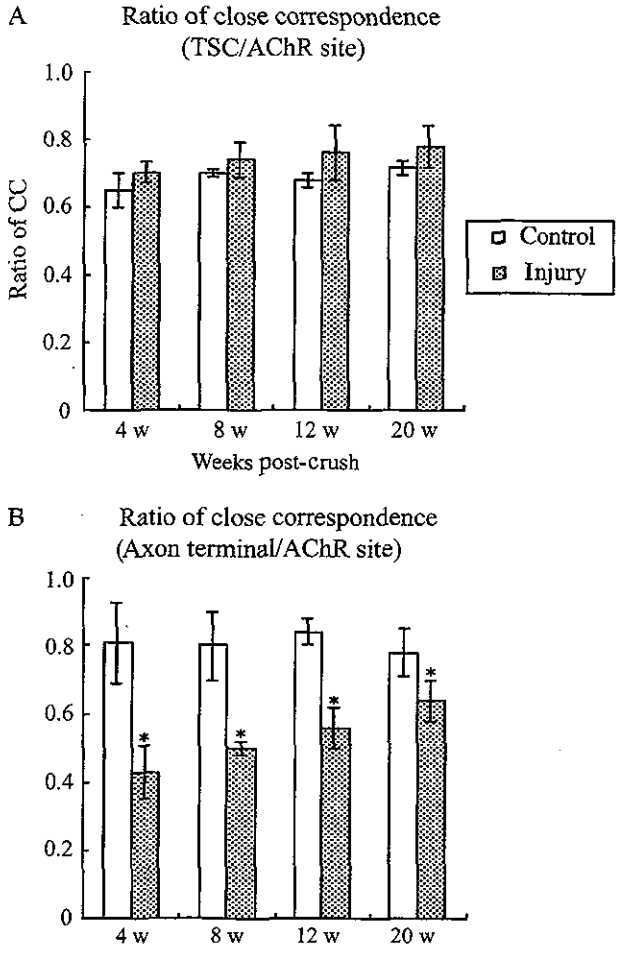

Figure 8. Available contact areas of neuromuscular junctions (NMJs) are estimated by the ratio of close correspondence (CC) at 4-, 8-, 12-, and 20-weeks post-crush (wpc). The ratio of CC is expressed by the quotient of the mean area (μm^2) of superposition from terminal Schwann cells (TSCs) or axon terminals divided by the mean area of acetylcholine receptor sites, respectively. (A, B) In controls, junctions are almost completely occupied and values of ratio of CC are stable around 0.7 (A) or 0.8 (B). (A) After injury, ratios of CC of TSC always appear a little greater than controls, though statistically insignificant. (B) In contrast to TSCs, ratios of CC of axon terminal at 4, 8 and 12 wpc are reduced. Despite gradual recovery, they are still less than normal levels at 20 wpc. *denotes statistically significant difference from the control values ($p < 0.001$).

plaques, estimated by the mean areas of superposition divided by mean areas of the AChR site, are shown in Fig. 8. After 4 wpc, values of TSCs both in control and injured models displayed constantly higher levels (>0.7), especially a persistent greater value of operated groups than controls (Fig. 8A), which was basically consistent with that seen in the rapid and smooth spatial realignment of regenerating NMJs as shown in Fig. 7. The ratios of CC of axon terminals showed a pronounced decline at 4 wpc (controls vs. axon terminals at 4 weeks, 0.82 vs. 0.42) with gradual return to control levels, indicating that the rate of reoccupation in axon terminals over the geometry of the AChR plaques was delayed.

Variability of data between the two independent researchers

In order to make the morphometric analyses of the area of CC and the incidences of anomalous endplate changes, the sections from each group at different time points were measured and analyzed by one investigator and then were examined independently once again by another investigator. There was no discernible difference in the measured data, and the minor discrepancy (3–7%) between these two independent observations was from the deviation in identification of the territory of the terminals, or the overlooking of faintly stained fine neural profiles arising from axon terminals or TSCs, which should be included as a positive count at last.

Discussion

Regenerative endplate growth coupled with remodeling

On the basis of the *in vivo* visualization study of reinnervating NMJs, Rich and Lichtman *(1989)* reported that the original endplate site was always the site of reinnervation and the reinnervating nerve occupied all of the original synaptic sites. Our recent study showed that the endplate regeneration proceeded under coordinating regeneration of TSCs, axon terminals, and receptor regions *(Kawabuchi et al., 2001)*. In the present study, examining the superposition of TSCs or axon terminals over receptor regions showed the precise reoccupation of former endplate sites by regenerated TSCs or axon terminals, within the territory of the receptor sites. The onset of endplate being reoccupied by regenerating SCs at 4 wpc coincides with the schedule that regenerating Schwann tubes and axons grow into the NMJ, and subsequent re-establishment of nerve-muscle contact is in process.

With increases of the superposition areas, a large proportion of the synapses' own terminal sprouts and endplates continue to be innervated by two or more distinct axons. In response to injury, NMJs enlarged due to multiple innervation and/or elaboration of the terminal arborization. Individual terminals sharing the polyaxonally innervated NMJs displayed some differences in superposition patterns, indicating discrepancy in the maturation process. The formation of multiple superpositions per NMJ may further confirm that the

size and complexity of axon terminals on individual endplates coincide with response for adaptation, remodeling, and maintenance of endplate structures documented for adult NMJs *(Barker and Ip, 1966; Cardasis and Padykula, 1981; Wernig and Herrera, 1986; Robbins and Polack, 1988)*. The major finding in this study is some characteristic profiles during endplate reoccupation and the difference in the regeneration pattern between TSCs and axon terminals, utilizing morphometric procedures of confocal 3D images for quantification of endplate reoccupation.

Characteristic morphological features during endplate reoccupation

On the endplate reoccupation, most of NMJs showed almost complete endplate realignment gradually after 4 wpc. We found some anomalous morphological features, especially in superposition between TSCs (or axon terminals) and AChR sites in NMJs, for example, occasional endplate vacancy (the area of the AChR site that has not reoccupied by regenerating axon terminals) with poorly developed synaptic contacts. Following nerve-crush injury, there was a moderate shrinkage of the AChR sites, which is consistent with the result reported by Csillik et al. *(1999)*. The subsequent events in this region denote coincidence of shrinkage and redifferentiation (reconstruction or new formation) within the same plaque *(Womble, 1986; Grady et al., 2000; Kawabuchi et al., 2001)*. The endplate realignment evidently commenced on the preexisting AChR plaques. After arriving at the endplate region, regenerating axon terminals appear to display some coordination in size and shape in superposition with the postsynaptic receptor regions *(Rich and Lichtman, 1989)*. Occasional endplate vacancy during the period of synapse realignment then suggests that a few conformational disorders, according to altered endplate geometry, may occur accidentally or transiently. Either the disproportionate growth rates between the pre- and postsynaptic regions or the poor growth of individual occupants are responsible for this disorder. In some NMJs, the AChR plaques may enlarge at a faster rate both laterally and longitudinally than the TSCs or axon terminals.

Early recovery of TSCs compared to axon terminals

In our previous study, we introduced the measure of overlap as calculated from the region of CC utilizing a dual-color confocal imaging technique *(Kawabuchi et al., 2001)*, the digitally subtracting procedure in the binary image for analysis of superimposed areas, as demonstrated in this communication. It is simple and repeatable and also useful to provide a reliable estimate of the extent of CC at the NMJ. As shown by the statistical data, the early recovery of the TSC-apposing contact areas compared to that of the axon terminals verifies differences in the regeneration patterns between these two endplate elements. It is potential that regeneration of the TSCs proceeds more rapidly at NMJs in order to reoccupy the postsynaptic receptor region sufficiently. In contrast, during the period of extensive growth of terminal branches in the synapse, the existing branches and bifurcation of motor nerve terminals elongated in a way that exactly matched the growth of receptor areas.

Normally, TSCs do not send processes into the synaptic gutter, and regeneration of the TSCs without invagination into the synaptic gutters may in part contribute to the early recovery of superposition areas in TSCs compared to axon terminals. Because TSCs engulf degenerating terminals and axons, and directly induce nerve terminal sprouts, they are likely to play important roles in facilitating successful reinnervation and regeneration in NMJs after nerve damage *(Son and Thompson, 1995a; 1995b; O'Malley et al., 1999; Kawabuchi et al., 2001)*. Certainly, adaptation to the synaptic environment during remodeling or regeneration is essential for TSCs to effectively modulate synaptic efficacy and neuronal activity *(Jahromi et al., 1992; Rochon et al., 2001)*. The rapid recovery in structures and superposition areas of TSCs after denervation suggests that they may be potential enough to exert a functional influence early in endplate reoccupation. Together with previous observations made using immunostaining *(Son and Thompson, 1995a; 1995b)*, the observations described here suggest that TSCs could be the substrate for nerve terminal and axon regeneration after nerve damage.

Anatomical relationship between presynaptic and postsynaptic elements

In development, the postsynaptic receptor region is an important determinant of endplate and terminal growth because postsynaptic regions grow at a faster rate than nerve terminals, and thus expansion of motor nerve terminals in NMJs is followed by postsynaptic growth *(Slack et al., 1983; Habgood and Hopkins, 1987)*. In regeneration, it has been suggested that receptors may be advantageous in the process of endplate reformation and may be in part important in the maintenance of regenerating nerve terminals, and that, in synaptic misalignment or their absence, nerve terminals are not maintained *(Rich and Lichtman, 1989; Balice-Gordon and Lichtman, 1990)*. In this study, a close correlation in the rates of size increase between the AChR sites and presynaptic elements suggests that the two elements are making alignment synchronously and reciprocally, and that the period when AChR sites progressively regenerate from shrinkage coincides with the period of growth of presynaptic elements. On the basis of this highly correlated

regeneration, we considered that the AChR site might be particularly important in promoting endplate regeneration. First, from early in reinnervation, pre-existing AChR sites provided the site where regeneration of TSCs and axon terminals proceeded. Secondly, it has been suggested that size increases in the developing postsynaptic site may initiate the growth of the axon terminal by some kind of contact-mediated interaction *(Nudell and Grinnel, 1983; Hopkins et al., 1985)*. In this study, the areas of CC and ratios of CC in TSCs or axon terminals represented the magnitudes of the spatial availability in relation to the AChR sites in regenerating NMJs. Indeed, we observed an ongoing recovery in this parameter of axon terminal- or TSC-mediated superposition. Finally, in our recent study, persistent damage of AChR sites was intimately associated with aging-related deterioration in reinnervation and regeneration of the endplates *(Kawabuchi et al., 2001)*. This evidence supports the possibility discussed above that the postsynaptic AChR sites contributed to the synaptic regeneration observed in NMJs. However, nerve injury primarily induces muscle atrophy, which accounts for not only decline of the trophic support for neurons but a reduction of neuronal support *(Johnson et al., 1995)*. Hence, it is important to note that a lot of evidence in recent years suggested that multiple cellular interactions between the pre- and postsyanptic elements, involving some local controls (via agrin, neuregulin, etc.), are necessary for synaptic reformation of the regenerating SCs, axons, and AChR sites in NMJs *(Kleiman and Reichardt, 1996; Denzer et al., 1997; Burden, 1998)*. This study does not address the possibility that the observed changes may provide direct and distinct proof for the synaptic interactions. However, on the basis of the frequent occurrence of unbalanced growth, for example, well-regenerated presynaptic regions contacting the malformed AChR sites (Figs. 4 and 5), the postsynaptic receptor region is unlikely to be an exclusive determinant for promoting endplate regeneration. It is concluded that a complex set of anatomical relationships between two or among the three endplate components affect the result of endplate reoccupation.

Persistent endplate reoccupation

We note that values of CC offer a tool to follow up the magnitude of morphological as well as potential physiological recovery in the pathway of reestablishment of synapse formation in regenerating NMJs. From ongoing recovery under lower CC values, we found persistent existence of incompletely occupied endplates, even up to 20 wpc. Anomalous synaptic disorder, such as greatly unoccupied AChR plaques and poorly formed individual occupants, was a consistent feature of these NMJs. This is compatible with the results from long-term observations on the pattern of reinnervation in which regenerated axons chronically exhibited pronounced morphological and physiological abnormalities for years *(Bowe et al., 1989)*. Following injury of peripheral nerves, the reasons for unsuccessful repair might come from two points, failure of axonal regeneration and the innervation of incorrect targets. The former derives from axon–SC interactions and other factors from peripheral glial cells, which are particularly important in nerve regeneration *(Ide et al., 1983; Scherer and Salzer, 1996)*. As for the latter, regenerating axons can cross endoneurial walls, even though the longitudinal continuity of these sheaths has been broken in crush lesions *(Brown and Hardman, 1987)*. Some mismatching is then possible when each proximal stump axon destines for its target via the endoneurial tube *(Fawcett and Keynes, 1990; Reynolds and Woolf, 1993)*. The establishment of precise spatial realignment could be a prerequisite to successful endplate regeneration. However, imperfect reinnervation and regeneration at the NMJ may give rise to sporadic remodeling during endplate reoccupation. Further investigation for the factors contributing to the mechanism of the spontaneous misalignment might be crucial in understanding the process in successful endplate regeneration.

Acknowledgements

We thank Mr. Takaaki Kanemaru (Morphology Core, Faculty of Medicine, Kyushu University) and Yasuhiro Hirakawa for their help in preparing photomicrographs. Grant Sponsor: Ministry of Education, Culture and Science of Japan; grant number: 12000210, 12670018 to M. K.

References

Balice-Gordon RJ, Lichtman JW (1990). In vivo visualization of the growth of pre- and postsynaptic elements of neuromuscular junctions in the mouse. J Neurosci 10:894–908.

Balice-Gordon RJ, Lichtman JW (1993). In vivo observations of pre- and postsynaptic changes during the transition from multiple to single innervation at developing neuromuscular junctions. J Neurosci 13:834–855.

Barker D, Ip MC (1966). Sprouting and degeneration of mammalian motor axons in normal and de-afferentated skeletal muscle. Proc R Soc Lond B Biol Sci 163:538–554.

Bowe CM, Hildebrand C, Kocsis JD, Waxman SG (1989). Morphological and physiological properties of neurons after long-term axonal regeneration: observations on chronic and delayed sequelae of peripheral nerve injury. J Neurol Sci 91:259–292.

Brown MC, Hardman VJ (1987). A reassessment of the accuracy of reinnervation by motoneurons following crushing or

freezing of the sciatic or lumbar spinal nerves of rats. Brain 110:695–705.
Burden SJ (1998). The formation of neuromuscular synapses. Genes Dev 12:133–148.
Cardasis CA, Padykula HA (1981). Ultrastructural evidence indicating reorganization at the neuromuscular junction in the normal rat soleus muscle. Anat Rec 200:41–59.
Crews LL, Wigston DJ (1990). The dependence of motoneurons on their target muscle during postnatal development of the mouse. J Neurosci 10:1643–1653.
Csillik B, Nemcsók J, Chase B, Csillik AE, Knyihár-Csillik E (1999). Infraterminal spreading and extrajunctional expression of nicotinic acetylcholine receptors in denervated skeletal muscle. Exp Brain Res 125:426–434.
Denzer AJ, Hauser DM, Gesemann M, Ruegg MA (1997). Synaptic differentiation: the role of agrin in the formation and maintenance of the neuromuscular junction. Cell Tissue Res 290:357–365.
Fawcett JW, Keynes RJ (1990). Peripheral nerve regeneration. Annu Rev Neurosci 13:43–60.
Glicksman MA, Sanes JR (1983). Differentiation of motor nerve terminals formed in the absence of muscle fibres. J Neurocytol 12:661–671.
Grady R, Zhou MH, Cunningham JM, Henry MD, Campbell KP, Sanes JR (2000). Maturation and maintenance of the neuromuscular synapse: genetic evidence for roles of the dystrophin–glycoprotein complex. Neuron 25:279–293.
Grinnell AD, Herrera AA (1981). Specificity and plasticity of neuromuscular connections: long term regulation of motoneuron function. Prog Neurobiol 17:203–282.
Habgood MD, Hopkins WG (1987). End-plate growth exceeds nerve terminal growth in juvenile mice. Exp Neurol 96:474–478.
Hall ZW, Sanes JR (1993). Synaptic structure and development: the neuromuscular junction. Cell 72:99–121.
Hirata K, Zhou C, Nakamura K, Kawabuchi M (1997). Postnatal development of Schwann cells at neuromuscular junctions, with special reference to synapse elimination. J Neurocytol 26:799–809.
Hopkins WG, Brown MC, Keynes RJ (1985). Postnatal growth of motor nerve terminals in muscles of the mouse. J Neurocytol 14:525–540.
Ide C, Tohyama K, Yokota R, Nitatori T, Onodera S (1983). Schwann cell basal lamina and nerve regeneration. Brain Res 288:61–75.
Jahromi BS, Robitale R, Charlton MP (1992). Transmitter release increases intracellular calcium in presynaptic Schwann cells in situ. Neuron 8:1069–1077.
Johnson H, Mossberg K, Arvidsson U, Piehl F, Hokfelt T, Ulfhake B (1995). Increase in alpha-CGRP and GAP-43 in aged motoneurons: a study of peptides, growth factors, and ChAT mRNA in the lumbar spinal cord of senescent rats with symptoms of hindlimb incapacities. J Comp Neurol 359:69–89.
Kawabuchi M, Zhou C, Islam ATM, Hirata K, Nada O (1998). The effect of aging on the morphological nerve changes during muscle reinnervation after nerve crush. Restor Neurol Neurosci 12:1–6.
Kawabuchi M, Zhou C, Wang S, Nakamura K, Liu WT, Hirata K (2001). The spatiotemporal relationship among Schwann cells, axons and postsynaptic acetylcholine receptor regions during muscle reinnervation in aged rats. Anat Rec 264:183–202.
Kleiman RJ, Reichardt LF (1996). Testing the agrin hypothesis. Cell 85:461–464.
Kuno M (1990). Target dependence of motoneuronal survival: the current status. Neurosci Res 9:155–172.
Navarro X, Verdu E, Wendelschafer-Crabb G, Kennedy WR (1997). Immunohistochemical study of skin reinnervation by regenerative axons. J Comp Neurol 380:164–174.
Nudell BM, Grinnell AD (1983). Regulation of synaptic position, size and strength in anuran skeletal muscle. J Neurosci 3:161–176.
O'Malley JP, Waran MT, Balice-Gordon RJ (1999). In vivo observations of terminal Schwann cells at normal, denervated, and reinnervated mouse neuromuscular junctions. J Neurobiol 38:270–286.
Reynolds ML, Woolf CJ (1993). Reciprocal Schwann cell-axon interactions. Curr Biol 3:683–693.
Rich MM, Lichtman JW (1989). In vivo visualization of pre- and postsynaptic changes during synapse elimination in reinnervated mouse muscle. J Neurosci 9:1781–1805.
Robbins N, Polak J (1988). Filopodia, lamellipodia and retractions at mouse neuromuscular junctions. J Neurocytol 17:545–561.
Rochon D, Rousse I, Robitaille R (2001). Synapse–glia interactions at the mammalian neuromuscular junction. J Neurosci 21:3819–3829.
Sanes JR (2003). The basement membrane/basal lamina of skeletal muscle. J Biol Chem 278: 12601–12604.
Sanes JR, Marshall LM, McMahan UJ (1978). Reinnervation of muscle fiber basal lamina after removal of myofibers. Differentiation of regenerating axons at original synaptic sites. J Cell Biol 78:176–198.
Scherer SS, Salzer JL (1996). Axon–Schwann cell interactions during peripheral nerve degeneration and regeneration. In: Glial Cell Development. Jessen KR, Richardson WD (Eds). Oxford Univeristy Press, London, Oxford, pp 165–196.
Slack JR, Pocket S, Macclement BAE (1983). Regulation of postnatal growth of motor endplates in rat soleus muscle. Exp Neurol 80:321–328.
Son YJ, Thompson WJ (1995a). Schwann cell processes guide regeneration of peripheral axons. Neuron 14:125–132.
Son YJ, Thompson WJ (1995b). Nerve sprouting in muscle is induced and guided by processes extended by Schwann cells. Neuron 14:133–141.
Trachtenberg JT, Thompson WJ (1997). Nerve terminal withdrawal from rat neuromuscular junctions induced by neuregulin and Schwann cells. J Neurosci 17:6243–6255.
Verdú E, Navarro X (1997). Comparison of immunohistochemical and functional reinnervation of skin and muscle after peripheral nerve injury. Exp Neurol 146:187–198.
Wernig A, Herrera AA (1986). Sprouting and remodeling at the nerve-muscle junction. Prog Neurobiol 27:251–291.
Womble MD (1986). The clustering of acetylcholine receptors and formation of neuromuscular junctions in regenerating mammalian muscle grafts. Am J Anat 176:191–205.

ELSEVIER

Journal of the Neurological Sciences 228 (2005) 87–92

Journal of the Neurological Sciences

www.elsevier.com/locate/jns

Th2 shift in juvenile muscular atrophy of distal upper extremity: a combined allergological and flow cytometric analysis

Manabu Osoegawa, Hirofumi Ochi, Feng-Jun Mei, Motozumi Minohara, Hiroyuki Murai, Takayuki Taniwaki, Jun-ichi Kira*

Department of Neurology, Neurological Institute, Graduate School of Medical Sciences, Kyushu University, Fukuoka 812-8582, Japan

Received 26 March 2004; received in revised form 1 October 2004; accepted 14 October 2004
Available online 24 November 2004

Abstract

Juvenile muscular atrophy of the distal upper extremity (JMADUE) is considered to be a type of flexion myelopathy; however, we recently reported cases of JMADUE associated with airway allergy successfully treated by plasma exchange. To further characterize the allergo-immunological features of JMADUE, 11 consecutive JMADUE patients in the neurology clinic at Kyushu University Hospital were studied. Past and present together with family histories of common allergic disorders were investigated. Total serum IgE was measured by an enzyme linked immunosorbent assay (ELISA) and allergen-specific IgE by a liquid phase enzyme immunoassay. Intracellular interferon (IFN) γ-, interleukin (IL)-4-, IL-5- and IL-13-producing T cells in peripheral blood were analyzed by flow cytometry. Data from 42 healthy subjects were used as controls for allergological studies. Flow cytometric data from 21 healthy subjects were also used for comparison. The patients exhibited significantly higher frequencies of coexisting airway allergies such as allergic rhinitis (p=0.0057) and pollinosis (p=0.0064), family histories of allergic disorders (p=0.0075), and mite antigen specific IgE (p=0.0361) compared with the healthy subjects. Patients with JMADUE had a significantly higher percentage of IFNγ$^-$IL-4$^+$CD4$^+$T cells (p=0.0017), but not IL-5- or IL-13-producing CD4$^+$T cells, and a reduced intracellular IFNγ/IL-4 ratio in CD4$^+$T cells (p=0.002) compared to the controls. These findings suggest that JMADUE has a significant T helper 2 (Th2) shift, which may in part contribute to the development of spinal cord damage.

Keywords: Flow cytometry; Hirayama disease; Atopy; IgE

1. Introduction

Juvenile muscular atrophy of the distal upper extremity (JMADUE), or Hirayama disease, is a rare disease that affects adolescents and is characterized by unilateral or asymmetric muscular atrophy and weakness in the hand and forearm [1,2]. The disease initially develops progressively, but is followed by spontaneous arrest several years after onset. The precise mechanism of this condition remains unclear, although contributing factors include a mechanical force pressing on the lower cervical cord and some microcirculatory deficiencies [1,3]. We have recently shown that this condition is closely associated with airway allergies, such as allergic rhinitis and bronchial asthma [4], and reported two cases associated with an airway allergy that were successfully treated by plasma exchange [5]. These reports indicate that atopy and its related immune aberration may contribute to the development of this condition.

In immune mediated diseases, the T helper 1 (Th1) and T helper 2 (Th2) cytokine balance plays a critical role [6]. The cytokine balance in JMADUE has not been reported. Therefore, in the present study, we aimed to determine the Th1/Th2 balance by flow cytometrically measuring the percentage of intracellular interferon (IFN)γ-, interleukin (IL)-4-, IL-5- and IL-13-producing T cells in peripheral blood CD4$^+$T cells and CD8$^+$T cells, and to clarify coexistent allergic conditions in 11 consecutive patients with JMADUE.

* Corresponding author. Tel.: +81 92 642 5340; fax: +81 92 642 5352.
E-mail address: kira@neuro.med.kyushu-u.ac.jp (J. Kira).

0022-510X/$ - see front matter © 2004 Elsevier B.V. All rights reserved.
doi:10.1016/j.jns.2004.10.003

2. Subjects and methods

2.1. Subjects

Eleven consecutive patients exhibiting JMADUE (two women and nine men, mean age 18 (range 13–22) years at the time of examination in the neurology clinic at Kyushu University Hospital) were enrolled in this study. Patients one through five were the same as those in a previous report [4].

2.2. Methods

Cervical MRI was performed in a neutral, and fully flexed position to examine the forward displacement of the dural sac and flattening of the lower cervical cord. All patients were questioned about their history of allergic disorders, such as bronchial asthma, allergic rhinitis, pollinosis, atopic dermatitis, allergic conjunctivitis, urticaria, and allergies to food, metals and drugs. Total serum IgE levels were measured by an enzyme linked immunosorbent assay (ELISA) and specific IgE to antigens such as *Dermatophagoides (D.) farinae*, *D. pteronyssinus*, cedar pollen, Candida, egg white, milk, wheat, rice, and soya bean were measured by a liquid phase enzyme immunoassay (Ala-STAT, Sankoujunyaku, Tokyo, Japan). A serum IgE concentration higher than 250 U/ml was considered to be hyperIgEaemia, and a cut off value for allergen specific IgE was set at 0.34 IU/ml in accordance with the manufacturer's instruction. The frequency of coexisting allergic disorders, hyperIgEaemia and allergen specific IgE, was determined by comparison with neurologically normal control data of 42 co-workers in the neurology clinic at Kyushu University Hospital, after obtaining their informed consent (mean age±S.D.=34.0±8.3 years, 22 male and 20 females).

Intracellular IFNγ, IL-4, IL-5 and IL-13 production from peripheral blood $CD4^+$ and $CD8^+$T cells were analyzed as described previously [7,8]. Briefly, peripheral blood-derived mononuclear cells were treated for 4 h with 25 ng/ml phorbol 12-myristate 13-acetate (Sigma, St. Louis, MO, USA) and 1 μg/ml of ionomycin (Sigma) in the presence of 10 μg/ml brefeldin A (Sigma). After washes with phosphate-buffered saline containing 0.1% bovine serum albumin (0.1% BSA-PBS), the cells were stained with PerCP-conjugated anti-CD4 (13B8.2, Becton Dickinson, San Jose, CA, USA) or anti-CD8 (1B9.2, Becton Dickinson) monoclonal antibody in the dark for 15 min at room temperature. Cells were washed twice, permeabilized with FACS permeabilizing solution (Becton Dickinson) and incubated with FITC-conjugated anti-IFNγ (clone 25723.11, Becton Dickinson) and PE-conjugated anti-IL-4 (clone 3010.211, Becton Dickinson), or either anti-IL-5 (JES1-39D10, PharMingen, San Diego, CA) or anti-IL-13 (JES10-5A2, PharMingen) monoclonal antibody in the dark at room temperature for 30 min. Corresponding isotype-matched antibodies were used as negative controls. As the last step, cells were washed with 0.1% BSA-PBS and resuspended in 1% paraformaldehyde for subsequent two-color flow cytometric analysis using an Epics XL System II (Coulter, Hialeah, FL, USA). Ten thousand events per lymphocyte were acquired and analyzed. Analysis gates were set on lymphocytes according to the forward and side scatter properties and then further gated on $CD4^+$ and $CD8^+$ cells, respectively. $CD8^+$ cells were divided into $CD8^{high}$ and $CD8^{low}$ [7]. Many $CD8^{low}$ cells expressed both CD16 and CD56 and, therefore, were considered to be natural killer cells. In contrast, virtually all $CD8^{high}$ cells expressed CD3 but not CD16 (data not shown). We therefore defined $CD8^{high}$ cells as $CD8^+$T cells. Flow cytometric data from patients with JMADUE was compared with data of 21 neurologically normal control subjects (30.5±6.2 years, 13 males and 9 females).

Statistical analysis for cell percentage comparison was performed using the Bonferroni/Dunn test with one-way factorial ANOVA. Either the chi-square test or Fisher's exact test (when the criteria of the chi-square test was not fulfilled) was used for the analysis of the frequency of atopic disorders, hyperIgEaemia and allergen-specific IgE.

3. Results

3.1. Clinical findings

During the 6-year analysis period, 11 consecutive patients (2 women and 9 men) exhibiting JMADUE were seen at our Institute (Table 1). The age of onset ranged from 12 to 18 years old (15.8±1.9), and the duration of the disease was 3 months to 7 years (2.5±1.9 years) at the time of examination. All showed gradual onset of unilateral or asymmetrical muscular atrophy and weakness in the distal parts of their upper extremities. Needle electromyogram revealed either on-going or chronic denervation potentials in the affected muscles of all patients. Cerebrospinal fluid examinations were all normal in the six patients who underwent lumbar puncture in our clinic. Cervical MRIs in a neutral position were normal, except for patient 6 who exhibited a high intense lesion in the left anterior horn on T2-weighted images at the C5-6 spine level not enhanced by gadolinium-DTPA. Cervical MRI in a fully flexed position of the neck showed 10 patients with a flattening of the lower cervical cord, but of these only six exhibited forward displacement of the dural sac together with an intense crescent-shaped signal behind the cord. One patient (patient 11) showed neither cord flattening nor a crescent-shaped signal. Two patients (patients 6 and 9) responded to plasma exchange and have been reported elsewhere [5].

Table 1
Clinical, allergological and MRI findings of patients with juvenile muscular atrophy of distal upper extremity

	Patient no.										
	1	2	3	4	5	6	7	8	9	10	11
Age at onset (years)	12	13	15	16	17	18	15	18	17	17	16
Age at examination (years)	13	15	22	17	19	19	15	20	20	22	19
Sex	F	F	M	M	M	M	M	M	M	M	M
Onset mode	Insidious	Insidious	Insidious	Insidious	Insidious	Insidious	Insidious	Insidious	Insidious	Insidious	Insidious
Muscle atrophy of distal upper extremity	R>L	R>L	R<L	R	R>L	R<L	R	R	R>L	R<L	R
Coexisting atopic/allergic disorders											
Bronchial asthma	+[a]	–	–	(+)[b]	–	–	–	–	–	–	(+)[b]
Allergic rhinitis	–	+	+	+	–	+	+	–	–	–	+
Pollinosis	–	–	+	–	–	–	–	+	+	+	+
Atopic dermatitis	–	–	–	–	–	–	(+)[b]	–	–	–	–
Others	+	–	–	–	–	+	+	+	+	+	–
Family history of atopic/allergic disorders	+	+	+	+	+	+	+	–	–	+	+
Peripheral blood eosinophil (%)[c]	7.8	7.6	2.7	4.5	6.7	5.2	5.3	4.4	14.2	2.0	8.3
Total serum IgE (IU/ml)	1874	1225	204	2400	150	220	242	<50	111	324	383
Allergen specific IgE (IU/ml)											
D. pteronyssinus	85.96	>100	9.19	>100	1.52	>100	6.75	–	–	–	44.02
D. farinae	90.66	>100	7.75	>100	2.63	>100	2.78	–	–	–	20.48
Cedar pollen	–	1.53	54.68	0.52	–	2.41	–	0.75	60.13	10.69	0.45
Soya bean	–	–	0.38	NE	–	–	–	–	1.19	0.45	–
Others	–	–	–	NE	–	–	–	–	Rice; 1.32	Wheat; 1.81	Wheat; 0.51
CSF cell count (/μl)	1	NE	NE	NE	NE	0	2	0	0	NE	0
CSF protein (mg/dl)	19	NE	NE	NE	NE	34	32	21	20	NE	17
Cervical MRI on flexion											
Cord flattening	+	+	+	+	+	+	+	+	+	+	–
Epidural venous dilatation	+	+	+	+	+	–	+	–	–	–	–

NE=not examined.
[a] Neurological symptoms developed gradually and were not related to asthma attacks.
[b] History of atopic/allergic disorders not present at the time of neurological illness is shown in parentheses.
[c] Eosinophil percentage higher than 4% is considered hypereosinophilia.

3.2. History of allergic disorders

The frequency of coexisting allergic disorders was significantly higher in patients with JMADUE than in the healthy control subjects (10/11 vs. 11/42, p=0.0002) (Fig. 1A). Of the patients, six (54.5%) had allergic rhinitis and five (45.5%) had pollinosis (Table 1), while in the normal control subjects, five (11.9%) had allergic rhinitis and three (7.1%) had pollinosis. The JMADUE group showed a significantly higher incidence of allergic rhinitis (p=0.0057) (Fig. 1B) and pollinosis (p=0.0064) (Fig. 1C). Two patients (patients 4 and 11) had a history of bronchial asthma that was not present at the time of their neurological illness. Although patient 1 had coexisting bronchial asthma when she developed JMADUE, the neurological symptoms developed gradually and were not related to the asthma attacks. None of the patients had coexisting atopic dermatitis but one (patient 7) had a history of atopic dermatitis that was not present at the time of their neurological illness. Nine of the eleven patients (81.8%) had a family history of allergic disorders in close relatives, and the frequency of a family history of allergic disorders was significantly greater in patients with JMADUE than in control subjects (5/42 (11.9%); p=0.0075) (Fig. 1D).

3.3. Allergological findings

Nine of the eleven patients (81.8%) showed mild to moderate eosinophilia (range 4.4% to 14.2%, normal<4.0%) in peripheral blood (Table 1). HyperIgEaemia was evident in five patients (45.5%), but the frequency of hyperIgEaemia was not significantly different between the patients with JMADUE and control subjects (12/42 (28.6%), p>0.1). All 11 patients had IgE specific for certain common allergens; 8 had IgE specific for two mite antigens, and 8 had IgE specific for cedar pollen. The frequency of mite antigen specific IgE was significantly higher in patients with JMADUE than in the control subjects (*D. pteronyssinus*, 8/11 vs. 14/42, p=0.0361; *D. farinae*, 8/11 vs. 14/42, p=0.0361) (Fig. 1E and F), but the frequency of cedar pollen specific IgE was not significantly different between the two groups (8/11 vs. 27/42, p>0.1).

3.4. Flow cytometric findings

The percentage of intracellular IFNγ$^+$IL-4$^-$CD4$^+$T cells in peripheral blood did not significantly differ between patients with JMADUE and control subjects (15.5±5.13 vs. 16.9±4.57) (Fig. 2A). The percentage of intracellular

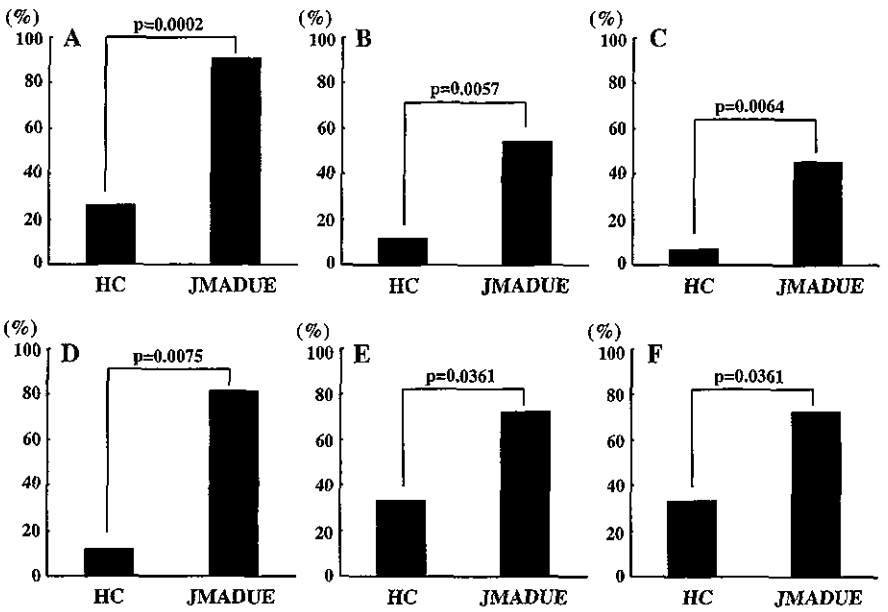

Fig. 1. Allergological features of juvenile muscular atrophy of the distal upper extremity. The frequencies of coexisting allergic disorders are shown: (A) total allergic disorders, (B) allergic rhinitis, (C) pollinosis, and a family history of allergic disorders (D). The frequency of mite antigen specific IgE is shown: (E) *D. pteronyssinus*, (F) *D. farinae*. The ordinate shows frequency in percentage. HC=healthy control subjects, JMADUE=juvenile muscular atrophy of the distal upper extremity.

IFNγ$^-$IL-4$^+$CD4$^+$T cells was significantly higher (2.73± 0.32 vs. 2.02±0.68, p=0.0017) (Fig. 2B) in patients with JMADUE compared to control subjects, and hence the intracellular IFNγ/IL-4 ratio in CD4$^+$T cells was significantly reduced (5.67±1.82 vs. 8.92±2.95, p=0.002) (Fig. 2C). There was no significant change in the percentages of either IFNγ$^+$IL-4$^-$ or IFNγ$^-$IL-4$^+$CD8$^+$T cells between the two groups. Neither IL-5$^+$ nor IL-13$^+$ cell percentages showed any significant changes between the two groups in either CD4$^+$ or CD8$^+$T cell fractions.

4. Discussion

This is the first flow cytometric study of JMADUE to show a Th2 shift in the immune balance. Moreover, the present study on a greater scale confirmed a previous observation that the frequency of coexisting airway allergies such as allergic rhinitis and pollinosis, a family history of allergic disorders, and mite antigen specific IgE was significantly higher in patients with JMADUE compared to healthy control subjects and indicated a

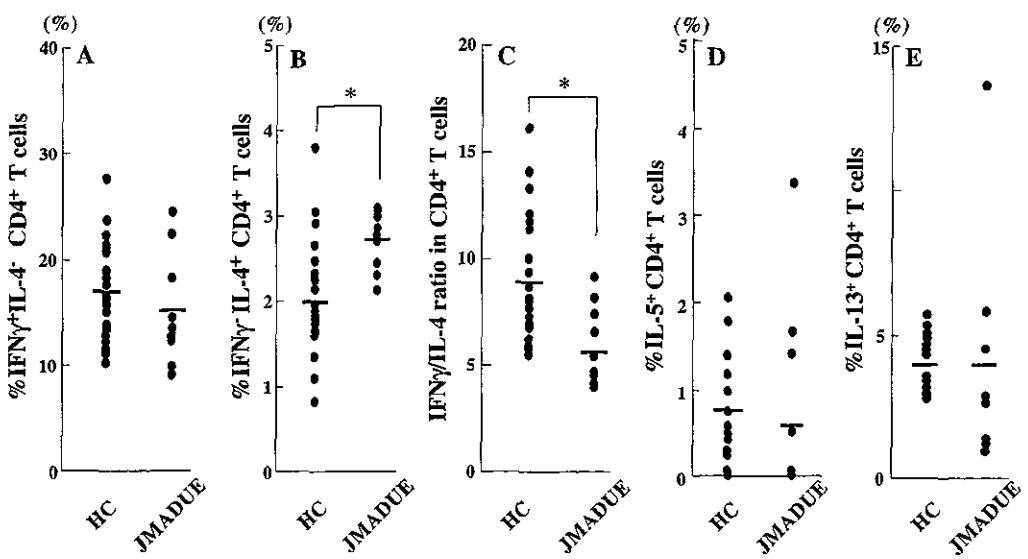

Fig. 2. Analysis of CD4$^+$T cell intracellular cytokine levels. The percentages of IFNγ$^+$IL-4$^-$ cells (A) and IFNγ$^-$IL-4$^+$ cells (B), IFNγ/IL-4 ratio (C) and the percentages of IL-5$^+$ cells (D) and IL-13$^+$ cells (E) in peripheral blood CD4$^+$T cells. *Statistically significant compared to healthy controls (p<0.01). The number of healthy controls in IL-5 and IL-13 assays is 16. HC=healthy control subjects, JMADUE=juvenile muscular atrophy of the distal upper extremity.

close association between atopic diathesis and JMADUE [4].

In this series, all patients displayed typical clinical features of JMADUE. Based on the radiological and neuropathological findings, repeated dynamic compression of the lower cervical cord followed by circulatory deficiencies may induce damage to the anterior horn cells, which are very vulnerable to ischemia [2,3]. However, neuroimaging showed that only 6 of the 11 patients exhibited flexion myelopathy, cervical cord flattening and epidural venous dilatation. Four patients showed mild cord flattening alone, and another had neither cord flattening nor forward displacement of the cervical dural sac. Other investigators have also failed to detect specific features of flexion myelopathy in some cases with this condition [9,10]. Furthermore, several investigators claim that such a forward displacement of the dural sac, and cord compression with neck flexion are even observed in normal people [9,11]. These findings indicate that JMADUE may be etiologically heterogeneous and that another mechanism other than flexion myelopathy may operate.

In the present study, we provide the first evidence of increases in the percentage of $IFN\gamma^{-}IL\text{-}4^{+}CD4^{+}T$ cells, and a reduction in the intracellular IFNγ/IL-4 ratio in $CD4^{+}T$ cells in JMADUE. Such a Th2 shift is consistent with hypereosinophilia and a heightened IgE response, which are frequently observed in this condition. It is well known that asthmatic amyotrophy (Hopkins syndrome), in which spinal motor neurons are affected, is also associated with atopic diathesis [12,13]. Thus airway allergy and related Th2 shift appear to contribute to cell damage of the spinal anterior horn of young people. On the other hand, we have reported occurrences of myelitis in patients with atopic dermatitis [14–16], naming it atopic myelitis. In this condition, the posterior column is preferentially involved. Although both JMADUE and atopic myelitis affect the cervical cord, involved sites on the axial plane of the spinal cord are distinct, i.e., anterior horns and posterior column, respectively. Therefore, both are considered to be distinct disease entities, yet both commonly have an allergic tendency and Th2 shift. It is interesting to note that atopic myelitis is preferentially associated with skin allergy whereas JMADUE and Hopkins syndrome are associated with airway allergy, thus suggesting a possibility that types of preceding atopic disorders may have some influence on the sites of involvement within the spinal cord.

Among the Th2 cytokines studied, IL-4, but not IL-5 or IL-13, was found to be upregulated in JMADUE. We previously reported that in atopic myelitis both IL-4 and IL-13 production was increased while IL-5 production was not elevated [7,17], and that opticospinal multiple sclerosis at relapse showed upregulation of IL-13 but neither IL-4 nor IL-5 [8]. The present findings together with the previous ones suggest that type 2 cytokine profiles are distinct among diseases affecting the spinal cord, and that in JMADUE IL-4 may play an important role. IL-4 is a key molecule for inducing a Th2 shift and allergic inflammation through a class switch from IgM to IgE [18], as well as stimulation for eotaxin synthesis [19]. Therefore, IgE-mediated activation of mast cells and/or eosinophils triggered by IL-4 [20] may be directly involved in spinal cord damage, or alternatively IL-4 may induce anti-neuronal autoantibodies that may damage spinal motor neurons. Human platelets can be activated by IgE and are therefore involved in the IgE-mediated effector mechanisms of allergic inflammation [21]. IgE-mediated activation of platelets causes platelet aggregation and histamine release, which may induce arterial spasm, as suggested by the increased incidence of circulatory deficiencies, such as cardiovascular diseases, in atopic patients [22–25]. It is possible that such a platelet-related disturbance of the circulatory system may also occur in JMADUE, in which IgE-mediated activation as well as repeated mechanical stress could be predisposing factors for platelet aggregation [26]. Plasma exchange, previously shown to be effective in some patients with JMADUE and airway allergy, may be beneficial by removing circulating factors, such as cytokines, IgE, autoantibodies and immune complexes. Another possibility is that allergic reaction and Th2 shift may be genetically linked to JMADUE, and have no direct involvement in anterior horn cell damage. However, as there have been no pathological studies of this disease during the early progressive stages, the nature of JMADUE remains unclear.

In summary, the numbers of Th2 cells were elevated in the peripheral blood of patients with JMADUE. The Th2 cytokine and IgE-mediated immune responses may contribute to the development of spinal cord damage in this condition, although comparison with patients with atopic diseases but without JMADUE will be required in the future. Further studies on cerebrospinal fluid cytokines are also called for to clarify the involvement of immunological processes in this condition.

Acknowledgements

This work was supported in part by a Neuroimmunological Disease Research Committee grant and a Research on Brain Science grant from the Ministry of Health and Welfare, Japan, and Grants-in-Aid 12557060 and 15590894 from the Ministry of Education, Science, Sports and Culture, Japan.

References

[1] Hirayama K, Tsubaki T, Toyokura Y, Okinaka S. Juvenile muscular atrophy of unilateral upper extremity. Neurology 1963;13:373–80.
[2] Hirayama K, Tokumaru Y. Cervical dural sac and spinal cord in juvenile muscular atrophy of distal upper extremity. Neurology 2000; 54:1922–6.
[3] Hirayama K, Tomonaga M, Kitano K, Yamada T, Kojima S, Arai K. Focal cervical poliopathy causing juvenile muscular atrophy of distal

upper extremity: a pathological study. J Neurol Neurosurg Psychiatry 1987;50:285–90.
[4] Kira J, Ochi H. Juvenile muscular atrophy of the distal upper limb (Hirayama disease) associated with atopy. J Neurol Neurosurg Psychiatry 2001;70:798–801.
[5] Ochi H, Murai H, Osoegawa M, Minohara M, Inaba S, Kira J. Juvenile muscular atrophy of distal upper extremity associated with airway allergy: two cases successfully treated by plasma exchange. J Neurol Sci 2003;206:109–14.
[6] Singh VK, Mehrotra S, Agarwal SS. The paradigm of Th1 and Th2 cytokines: its relevance to autoimmunity and allergy. Immunol Res 1999;20:147–61.
[7] Ochi H, Wu XM, Osoegawa M, Horiuchi I, Minohara M, Murai H, et al. Tc1/Tc2 and Th1/h2 balance in Asian and Western types of multiple sclerosis, HTLV-1-associated myelopathy/tropical spastic paraparesis and hyperIgEaemic myelitis. J Neuroimmunol 2001; 119:297–305.
[8] Ochi H, Osoegawa M, Wu X-M, Minohara M, Horiuchi I, Murai H, et al. Increased IL-13 but not IL-5 production by CD4-positive T cells and CD8-opsitive T cells in multiple sclerosis during relapse phase. J Neurol Sci 2002;201:45–51.
[9] Schroder R, Keller E, Flacke S, Schmidt S, Pohl C, Klockgether T, et al. MRI findings in Hirayama's disease: flexion-induced cervical myelopathy or intrinsic motor neuron disease? J Neurol 1999; 246:1069–74.
[10] Willeit J, Kiechl S, Kiechl-Kohlendorfer U, Golaszewski S, Peer S, Poewe W. Juvenile asymmetric segmental spinal muscular atrophy (Hirayama's disease): three cases without evidence of "flexion myelopathy". Acta Neurol Scand 2001;104:320–2.
[11] Robberecht W, Aguirre T, Van den Bosch L, Theys P, Nees H, Cassiman JJ, et al. Familial juvenile focal amyotrophy of the upper extremity (Hirayama disease). Superoxide dismutase 1 genotype and activity. Arch Neurol 1997;54:46–50.
[12] Mizuno Y, Komori S, Shigetomo R, Kurihara E, Tamagawa K, Komiya K. Poliomyelitis-like illness after acute asthma (Hopkins' syndrome). Brain Dev 1995;17:126–9.
[13] Horiuchi I, Yamasaki K, Osoegawa M, Ohyagi Y, Okayama A, Kurokawa T, et al. Acute myelitis after asthma attacks with onset after puberty. J Neurol Neurosurg Psychiatry 2000;68:665–8.
[14] Kira J, Yamasaki K, Kawano Y, Kobayashi T. Acute myelitis associated with hyperIgEemia and atopic dermatitis. J Neurol Sci 1997;148:199–203.
[15] Kira J, Kawano Y, Yamasaki K, Tobimatsu S. Acute myelitis with hyperIgEaemia and mite antigen specific IgE: atopic myelitis. J Neurol Neurosurg Psychiatry 1998;64:676–9.
[16] Kira J, Kawano Y, Horiuchi I, Yamada T, Imayama S, Furue M, et al. Clinical, immunological and MRI features of myelitis with atopic dermatitis (atopic myelitis). J Neurol Sci 1999;162:56–61.
[17] Ochi H, Osoegawa M, Murai H, Wu X-M, Taniwaki T, Kira J. Presence of IgE antibodies to bacterial superantigens and increased IL-13-producing T cells in myelitis with atopic diathesis. Int Arch Allergy Immunol 2004;134:41–8.
[18] Gauchat JF, Lebman DA, Coffman RL, Gascan H, de Vries JE. Structure and expression of germline ε transcripts in human B cells induced by interleukin 4 to switch to IgE production. J Exp Med 1990;172:463–73.
[19] Lezcano-Meza D, Dávila-Dávila B, Vega-Miranda A, Negrete-García LM, Teran LM. Interleukin (IL)-4 and to a lesser extent either IL-13 or interferon-gamma regulate the production of eotaxin-2/CCL24 in nasal polyps. Allergy 2003;58:1011–7.
[20] Katayama I, Tanei R, Yokozeki H, Nishioka K, Dohi Y. Induction of eczematous skin reaction in experimentally anti-DNP IgE antibody: possible implications for skin lesion formation in atopic dermatitis. Int Arch Allergy Appl Immunol 1990;93:148–54.
[21] Hasegawa S, Pawankar R, Suzuki K, Nakahata T, Furukawa S, Okumura K, et al. Functional expression of the high affinity receptor for IgE (FcepsilonRI) in human platelets and its' intracellular expression in human megakaryocytes. Blood 1999;93:2543–51.
[22] Knauer KA, Lichtenstein LM, Adkinson Jr NF, Fish JE. Platelet activation during antigen-induced airway reactions in asthmatic subjects. N Engl J Med 1981;304:1404–7.
[23] Criqui MH, Lee ER, Hamburger RN, Klauber MR, Coughlin SS. IgE and cardiovascular disease. Results from a population-based study. Am J Med 1987;82:964–8.
[24] Brunekreef B, Hoek G, Fischer P, Spieksma FT. Relation between airborne pollen concentrations and daily cardiovascular and respiratory-disease mortality. Lancet 2000;355:1517–8.
[25] Ginsburg R, Bristow MR, Kantrowitz N, Baim DS, Harrison DC. Histamine provocation of clinical coronary artery spasm: implications concerning pathogenesis of variant angina pectoris. Am Heart J 1981;102:819–22.
[26] Jesty J, Yin W, Perrotta P, Bluestein D. Platelet activation in a circulating flow loop: combined effects of shear stress and exposure time. Platelets 2003;14:143–9.

ELSEVIER

Journal of the Neurological Sciences 228 (2005) 75–85

Journal of the Neurological Sciences

www.elsevier.com/locate/jns

Th1 shift in CIDP versus Th2 shift in vasculitic neuropathy in CSF

Feng-Jun Mei, Takaaki Ishizu, Hiroyuki Murai, Manabu Osoegawa, Motozumi Minohara, Kun-Nan Zhang, Jun-ichi Kira*

Department of Neurology, Neurological Institute, Graduate School of Medical Sciences, Kyushu University, 3-1-1 Maidashi, Higashi-ku, Fukuoka 812-8582, Japan

Received 17 July 2004; received in revised form 1 October 2004; accepted 6 October 2004
Available online 12 November 2004

Abstract

To investigate the intra- and extracellular levels of various cytokines and chemokines in CSF in chronic inflammatory demyelinating polyneuropathy (CIDP) and vasculitic neuropathy (VN), 16 cytokines, IL-1β, IL-2, IL-4, IL-5, IL-6, IL-7, IL-8, IL-10, IL-12 (p70), IL-13, IL-17, IFN-γ, TNF-α, G-CSF, MCP-1 and MIP-1β, were measured in CSF supernatant by a multiplexed fluorescent bead-based immunoassay and intracellular production of IFN-γ and IL-4 in CSF $CD4^+$ T cells were simultaneously measured by flow cytometry in 14 patients with CIDP, 8 patients with VN and 25 patients with other noninflammatory neurologic diseases (OND). In the CSF supernatant, a significant increase of IL-17, IL-8 and IL-6, and a significant decrease of IL-4, IL-5 and IL-7 levels were detected in pretreated CIDP as compared with OND. A significant increase of IL-6, IL-8 and IL-10 levels was found in pretreated VN. Both IL-17 and IL-8 levels correlated strongly with CSF protein levels in CIDP, although the correlation of IL-6 levels was weak. In CSF $CD4^+$ T cells, IFN-γ^+ IL-4^- cell percentages were markedly elevated in CIDP compared with OND, but not in VN, resulting in a significant increase of intracellular IFN-γ/IL-4 ratio in CIDP, even in the absence of CSF pleocytosis. The nonresponders to intravenous immunoglobulins (IVIGs) showed a significantly lower IFN-γ^- IL-4^+ $CD4^+$ T cell percentage, and tended to have a higher intracellular IFN-γ/IL-4 ratio than the responders in CSF. Marked upregulation of Th1 cytokine, IL-17, and downregulation of Th2 cytokines, together with infiltration of IFN-γ-producing $CD4^+$ T cells are useful markers for CIDP, while several Th2 cytokines are upregulated in VN in CSF.

Keywords: Th1; Th2; CSF; Cytokine; CIDP; Vasculitic neuropathy

1. Introduction

Chronic inflammatory demyelinating polyneuropathy (CIDP) is regarded as an autoimmune disease targeting peripheral nerve myelin, although its mechanism remains unknown. Immunohistochemical studies of biopsied sural nerves revealed that both $CD4^+$ and $CD8^+$ T cells infiltrated together along with activated macrophages but without either B cells or immunoglobulin deposition [1,2], suggesting a critical role for T cells. On the other hand, humoral immunity, such as immunoglobulins and immune complexes, is believed to be involved in vasculitic neuropathy (VN) [3].

Chemokines are crucial for recruiting T cells to inflammatory sites. Recent studies on chemokines in CIDP CSF revealed an increase in chemokines, attracting mainly Th1 cells, such as CXCL10 (IP-10) [4,5], which coincides with the highest expression of CXCR3. CXCR3 is a chemokine receptor for CXCL10 and is specific for Th1 cells among chemokine receptors in the invading T cells in biopsied sural nerves [4]. However, the significance of the increase in chemokines in CSF still remains unclear, as there is no CSF pleocytosis in CIDP, and none of the studies found any changes in the cellular composition of CSF in this condition.

Moreover, in CIDP CSF, cytokines such as IL-1α, IL-1β, IL-2, IL-6, IL-10, IFN-γ, TNF-α and monocyte colony-stimulating factor (M-CSF) were all found to be negative by an enzyme-linked immunosorbent assay (ELISA) [6], except for in one earlier study that showed an increase of

* Corresponding author. Tel.: +81 92 642 5340; fax: +81 92 642 5352.
E-mail address: kira@neuro.med.kyushu-u.ac.jp (J. Kira).

0022-510X/$ - see front matter © 2004 Elsevier B.V. All rights reserved.
doi:10.1016/j.jns.2004.10.001

IL-6 [7]. However, a fluorescent bead-based immunoassay, with a wide dynamic range of standard curves, for multiple cytokines has become available, and requires only small amounts of materials for simultaneous measurements of multiple cytokines [8,9]. Therefore, the present study aimed to directly measure the intracellular cytokine production of $CD4^+$ T cells by flow cytometry, and various cytokine and chemokine levels of the CSF supernatant by multiplexed fluorescent bead-based immunoassay in CIDP and vasculitic neuropathy (VN). This was done to clarify the distinct immune balance in the CSF compartment. In addition, since CSF is considered to reflect events within the blood nerve barrier (BNB) more than in peripheral blood, we wanted to determine clinically useful CSF markers for each inflammatory neuropathy.

2. Materials and methods

2.1. Subjects

Fourteen patients with probable CIDP (9 males and 5 females, mean age±S.D.=60.1±17.2 years, range 28–80) based on the criteria of the American Academy of Neurology AIDS Task Force, were enrolled in this study [10]. In addition, 8 patients with untreated VN presented as mononeuritis multiplex (4 males and 4 females, mean age±S.D.=48.1±16.1 years, range 19–66) and 25 patients with other noninflammatory neurologic diseases (OND; 14 males and 11 females, mean age±S.D.=56.5±14.7 years, range 20–80) were also enrolled in the study. The OND group was composed of 14 patients with spinocerebellar degeneration, 2 with amyotrophic lateral sclerosis, 2 with cervical spondylosis, 2 with Alzheimer's disease and 1 each with Parkinson's disease, progressive supranuclear palsy, myelopathy, spinal cord infarction and epilepsy. The duration of CIDP ranged from 2 months to 24 years (mean±S.D.=6.69±8.95 years) at the time of lumbar puncture. Clinical courses were chronic progressive in 7, relapsing–remitting in 6 and monophasic in 1. Hughes grades [11] were 2 to 4 (mean±S.D.=3.21±0.89). All patients with CIDP showed motor dominant involvement and all but three showed symmetrical involvement. Eleven patients were treated by intravenous immunoglobulin (IVIG; 0.4g/kg/day) infusion for 5 days, and the six who improved by one or more than one grade on the Hughes scale after therapy were considered to be responders (Table 1).

2.2. Sample collection

At least 5 ml each of CSF and blood samples were obtained from all patients. In the case of CIDP, 26 CSF samples from 14 patients, 19 pretreatment and 7 posttreatment were obtained; all 8 CSF samples from the 8 VN patients were those from pretreatment. CSF samples were immediately centrifuged at 800 rpm/min at 4 °C for 5 min. The CSF cell counts in the samples used for the intracellular cytokine analysis were 2.0±1.0/μl (mean±S.D., range 1.0–4.0) in CIDP patients, 5.0±4.0/μl (mean±S.D., range 1.0–12.0) in VN patients and 1.0±0.5/μl (mean±S.D., range 1.0–2.0) in OND patients. CSF supernatant was kept under −70 °C until the cytokine assay.

2.3. Multiplexed fluorescent bead-based immunoassay

CSF supernatants were collected and analyzed simultaneously for 16 different cytokines and chemokines, namely, IL-1β, IL-2, IL-4, IL-5, IL-6, IL-7, IL-8, IL-10, IL-12 (p70), IL-13, IL-17, IFN-γ, TNF-α, granulocyte colony-stimulating factor (G-CSF), monocyte chemoattractant protein 1 (MCP-1) and macrophage inflammatory protein 1β (MIP-

Table 1
Demographic features of patients with CIDP

Patient no.	Age at onset (year)	Age at examination (year)	Sex	Duration	Hughes grade at peak	CSF cells/protein (/μl, mg/dl)	Clinical course	Response to IVIG	Clinical symptoms	
									Predominant symptoms	Symmetrical involvement
1	58	65	M	7 y	2	2/148	relapsing	good	motor>sensory	+
2	72	72	F	2 m	2	1/28	monophasic	good	motor>sensory	–
3	27	28	M	1 y	4	2/87	relapsing	good	motor>>sensory	+
4	58	59	F	4 m	2	4/69	relapsing	good	motor>>sensory	+
5	75	77	F	3 y	4	1/253	CP	good	motor>sensory	+
6	49	53	M	4 y	4	1/39	CP	good	motor>>sensory	+
7	79	80	M	1 y	4	2/36	CP	poor	motor>>sensory	+
8	75	76	F	1 y	4	4/45	CP	poor	motor>>sensory	–
9	40	64	M	24 y	4	2/102	CP	poor	motor>sensory	+
10	60	80	M	20 y	4	2/68	relapsing	poor	motor>sensory	+
11	37	39	M	2 y	2	1/72	CP	poor	motor>sensory	+
12	12	36	M	24 y	3	1/30	relapsing	NE	motor	+
13	46	46	M	2 m	3	1/127	CP	NE	motor>sensory	+
14	61	67	F	6 y	3	0/30	relapsing	NE	motor	–

CIDP: chronic inflammatory demyelinating polyneuropathy, M: male, F: female, m: months, y: years, CSF: cerebrospinal fluid, IVIG: intravenous immunoglobulin, CP: chronic progressive, NE: not examined.

1β) using the Bio-Plex Cytokine Assay System (Bio-Rad Laboratories, Hercules, CA) according to the manufacturer's instructions [8,9]. Briefly, 50 μl of each CSF supernatant and various concentrations of each cytokine standard (Bio-Rad) were added to 50 μl of antibody-conjugated beads (Bio-Rad) in a 96-well filter plate (Millipore, Billerica, MA). After a 30-min incubation, the plate was washed and 25 μl of a biotinylated antibody solution (Bio-Rad) was added to each well, followed by another 30-min incubation. The plate was then washed and 50 μl of streptavidin-conjugated PE (Bio-Rad) was added to each well and incubated for 10 min. Following a final wash, the contents of each well were resuspended in 125 μl of the assay buffer (Bio-Rad) and analyzed using a Bio-Plex Array Reader (Bio-Rad). The cytokine concentrations were calculated by reference to a standard curve for each cytokine derived using various concentrations of the cytokine standards (0.2, 0.78, 3.13, 12.5, 50, 200, 800 and 3200 pg/ml) assayed in the same manner as the CSF samples. The detection limit of each cytokine was determined by the recovery of the corresponding cytokine standard, and the lowest values showing more than 50% recovery were set as the lower detection limits. The lower detection limit for each cytokine was as follows: 0.2 pg/ml for IL-2, IL-4, IL-5, IL-7, IL-8, IL-10, IL-12 (p 70), IL-13, IL-17, IFN-γ and TNF-α, 0.78 pg/ml for IL-1β and IL-6, and 3.13 pg/ml for G-CSF, MCP-1 and MIP-1β. All samples were analyzed undiluted in duplicate. CSF supernatants used for the multiplexed fluorescent bead-based immunoassay were 26 CIDP (19 pre- and 7 posttreatment), 8 VN and 24 OND samples.

2.4. Intracellular cytokine analysis by flowcytometry

Each CSF supernatant was carefully removed and cell sediments were suspended in RPMI 1640 (Nipro, Tokyo, Japan) supplemented with 10% fetal calf serum (FCS; Gibco BRL, Gaithersburg, MD; Lot#3217341S). This was followed by incubation with 25 ng/ml of phorbol 12-myristate 13-acetate (PMA; Sigma, St. Louis, MO), 1.0 μg/ml of ionomycin (Sigma) and 10 μg/ml of Brefeldin A (BFA; Sigma) in a 24-well plate at 37 °C for 4 h under 5% CO_2. After washing with phosphate-buffered saline containing 0.1% bovine serum albumin (0.1% BSA-PBS), cells were stained with perCP-conjugated anti-CD4 monoclonal antibodies (Immunotech, Marseille, France) and incubated on ice in the dark for 15 min. Following another wash with 0.1% BSA-PBS, FACS permeabilizing solution (Becton Dickinson, San Jose, CA) was added and the cells were placed in the dark for 10 min. After two washes with 0.1% BSA-PBS, the cells were then stained with FITC-conjugated anti-IFN-γ (Immunotech) and PE-conjugated anti-IL-4 (Immunotech) for intracellular cytokine analysis, with mouse IgG2a-FITC (Immunotech) and IgG1-PE (Immunotech) as controls. After a 30-min incubation on ice in the dark, the percentages of intracellular IFN-γ-and IL-4-producing cells were immediately analyzed flowcytometrically using an Epics XL System II (Coulter, Hialeah, FL). Analysis gates were first set on lymphocytes according to the forward and side scatter properties and then set on $CD4^+$ lymphocytes. Cases with $CD4^+$ cell counts of less than 500 were discarded from the analysis to increase the reliability. For peripheral blood lymphocytes (PBL), intracellular cytokines were studied as described previously [12], using the same amounts of PMA, ionomycin and BFA, and the same monoclonal antibodies for staining. CSF cells taken from 10 patients with pretreated CIDP, 8 with VN at the pretreatment time and 12 OND patients, were used for intracellular cytokine analysis.

2.5. Statistical analysis

Statistical analyses were performed by the nonparametric Mann–Whitney *U* test to determine the significance between OND and each disease group. The difference between CSF and PBL in each group was analyzed by Wilcoxon signed rank test. In the CIDP group, the difference between responders and nonresponders was also analyzed by Mann–Whitney *U* test.

3. Results

3.1. Detection rates of each cytokine in CSF supernatant

The detection rate of IL-17 was significantly higher in pretreated CIDP patients compared with OND patients (19/19, 100% vs. 11/24, 45.8%, p=0.0004) and that of IL-10 was also significantly higher in VN patients (8/8, 100% vs. 11/24, 45.8%, p=0.0104), while that of IL-4 was significantly lower in pretreated and posttreated CIDP patients (10/19, 52.6% vs. 23/24, 95.8%, p=0.0022 and 3/7, 42.9% vs. 23/24, 95.8%, p=0.0051, respectively; Fig. 1). The detection rates of other cytokines were not significantly different between OND patients and each disease condition. IL-2 and IL-12 (p70) were not used for further statistical analyses because of low detection rates in CSF.

3.2. Comparison of cytokine levels in CSF supernatant among diseases

In CIDP patients, IL-17, IL-8 and IL-6 levels were significantly increased at the time of pretreatment as compared with OND levels (10.32±7.69 vs. 4.39±6.02 for the mean±S.D. and 10.33 vs. 0.19 for the median, p=0.0019; 31.17±19.99 vs. 14.23±9.20 and 25.50 vs. 11.32, p=0.0020; 42.94±27.82 vs. 62.89±179.80 and 30.29 vs. 21.55, p=0.0060, respectively; Fig. 2). After IVIG, the increase of IL-8 levels was still significant (31.62±12.26 vs. 14.23±9.29 and 32.00 vs. 11.32, p=0.0025) but not those of IL-17 (9.59±6.50 vs. 4.39±6.02 and 9.22 vs. 0.19) and IL-6 (44.94±26.26 vs. 62.89±179.77 and 31.95 vs. 21.55). In contrast, IL-4, IL-5

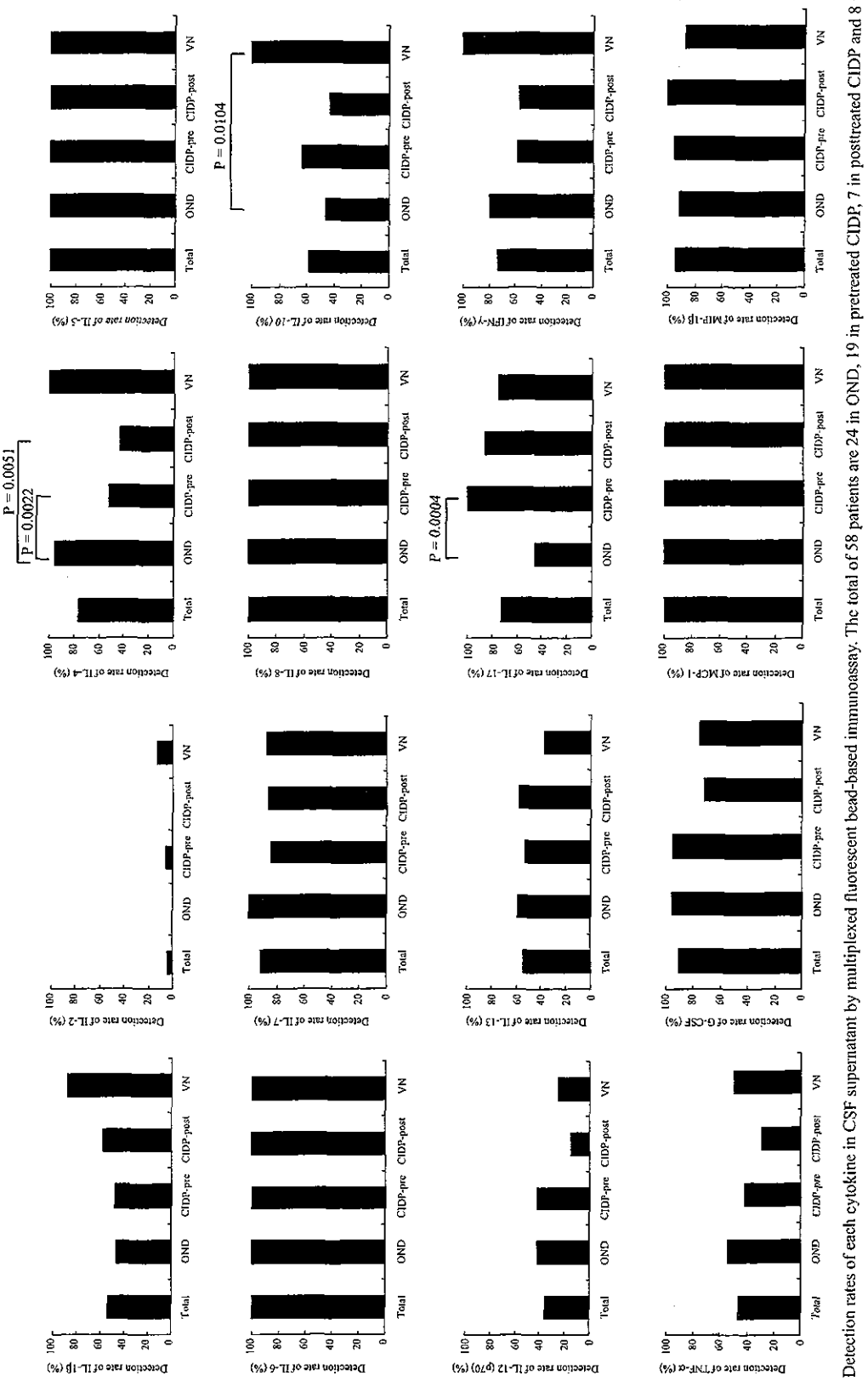

Fig. 1. Detection rates of each cytokine in CSF supernatant by multiplexed fluorescent bead-based immunoassay. The total of 58 patients are 24 in OND, 19 in pretreated CIDP, 7 in posttreated CIDP and 8 in VN.

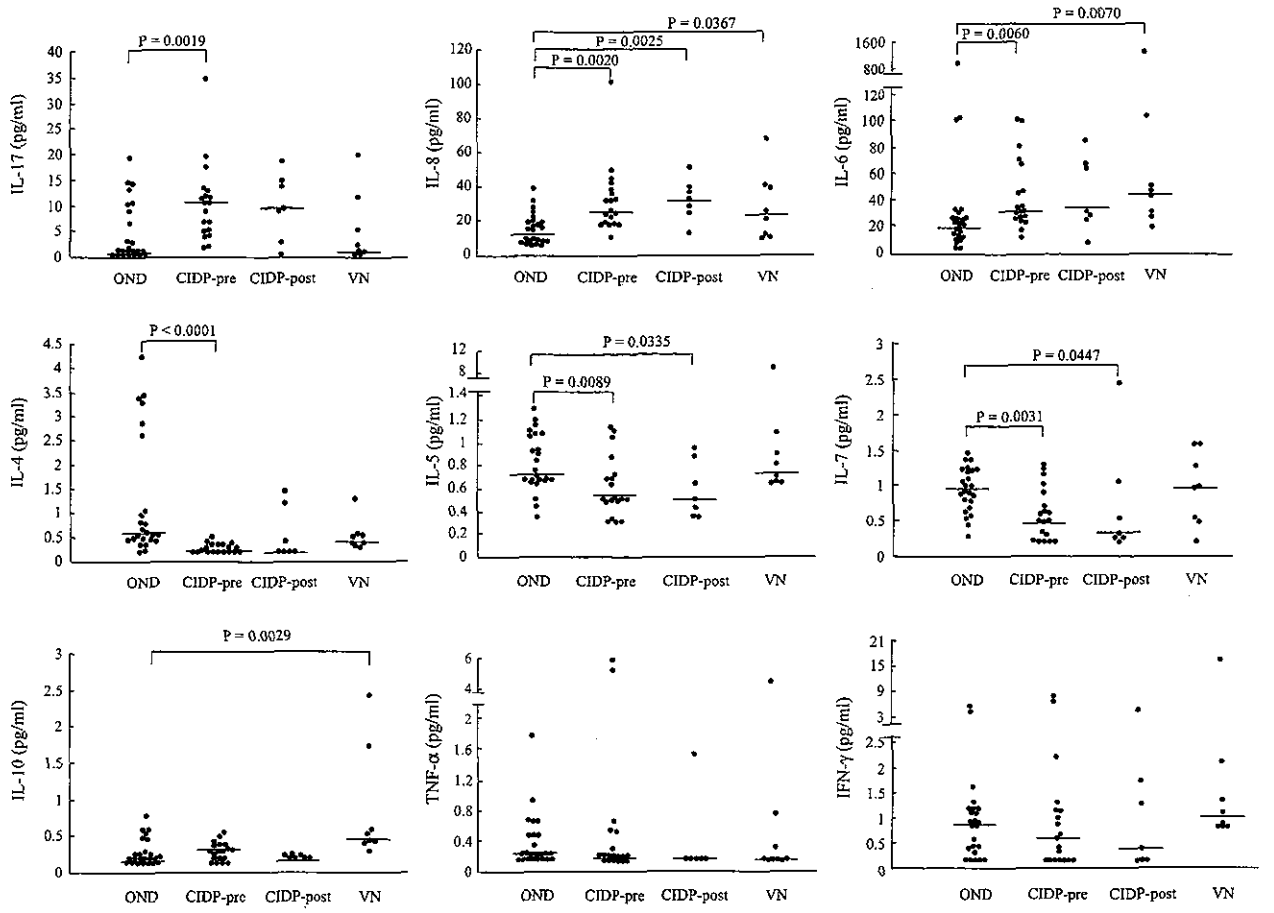

Fig. 2. Cytokine levels in the CSF supernatant in OND, CIDP and VN by multiplexed fluorescent bead-based immunoassay. CIDP-pre=CIDP at the pretreatment. CIDP-post=CIDP after the IVIG (6 patients were responders and 5 nonresponders). IL-1β, IL-13, G-CSF, MCP-1 and MIP-1β are not shown in the figure, but mean±S.D. and median values of these cytokines are given in the text. IL-2 and IL-12 (p70) are not shown due to the low detection frequency in CSF.

and IL-7 levels were significantly decreased at pretreatment (0.27±0.09 vs. 1.22±1.26 and 0.22 vs. 0.55, $p<0.0001$, 0.62±0.26 vs. 0.82±0.25 and 0.57 vs. 0.74, $p=0.0089$, and 0.58±0.36 vs. 0.94±0.31 and 0.48 vs. 0.95, $p=0.0031$, respectively). At the time of posttreatment, decreases of IL-5 and IL-7 levels were still significant (0.59±0.24 vs. 0.82±0.25 and 0.52 vs. 0.74, $p=0.0335$, and 0.72±0.81 vs. 0.94±0.31 and 0.31 vs. 0.95, $p=0.0447$, respectively) but this was not the case for IL-4 levels (0.54±0.53 vs. 1.22±1.26 and 0.19 vs. 0.55). None of the other cytokines or chemokines showed any significant changes at either the pre- or posttreatment times. The concentrations of the other cytokines and chemokines, which did not show any significant changes, were as follows in the pretreatment CIDP, posttreatment CIDP and OND patients: IL-1β (pg/ml), 1.55±1.11 (mean±S.D.) and 0.77 (median), 2.25±2.56 and 0.93, and 1.36±0.73 and 0.77; IL-13 (pg/ml), 0.77±1.05 and 0.20, 0.9±1.55 and 0.34, and 0.65±0.76 and 0.24; IFN-γ (pg/ml), 1.47±2.55 and 0.53, 1.16±1.47 and 0.43, and 1.05±1.18 and 0.81; G-CSF (pg/ml), 33.24±29.61 and 21.11, 14.74±9.70 and 18.20, and 25.35±21.50 and 19.85; MCP-1 (pg/ml), 219.05±154.72 and 169.71, 145.97±89.18 and 99.55, and 174.3±69.31 and 160.32; MIP-1β (pg/ml), 11.05±6.3 and 10.80, 13.31±7.9 and 12.79, and 16±13.85 and 10.28; IL-10, (pg/ml) 0.29±0.11 and 0.29, 0.21±0.02 and 0.19, and 0.30±0.17 and 0.19; TNF-α (pg/ml) 0.80±1.64 and 0.19, 0.42±0.46 and 0.19, and 0.36±0.32 and 0.20, respectively.

In contrast, VN patients showed a significant increase of IL-6, IL-8 and IL-10 levels as compared with OND patients at the time of pretreatment (208.54±457.09 vs. 62.89±179.77 and 43.41 vs. 21.55, $p=0.0070$, 27.52±20.30 vs. 14.23±9.29 and 22.53 vs. 11.32, $p=0.0367$, and 0.85±0.78 vs. 0.30±0.17 and 0.48 vs. 0.19, $p=0.0029$, respectively). There were no significant changes in concentration of any of the other cytokines and chemokines in VN patients, and the results are as follows: IL-1β (pg/ml), 1.63±1.52 (mean±S.D.) and 1.16 (median); IL-4 (pg/ml), 0.53±0.33 and 0.44; IL-5 (pg/ml), 1.80±2.91 and 0.75; IL-7 (pg/ml), 0.94±0.52 and 0.95; IL-13 (pg/ml), 0.64±0.75 and 0.19; IL-17 (pg/ml), 5.07±7.07 and 1.58; IFN-γ (pg/ml), 2.98±5.45 and 1.0; TNF-α (pg/ml), 0.77±1.41 and 0.20; G-CSF (pg/ml), 30.52±22.55 and 35.02; MCP-1 (pg/ml), 182.22±96.40 and 169.82; MIP-1β (pg/ml), 9.47±5.04 and 6.67.